Seismic scattering property changes correlate with ground deformation at Suwanosejima volcano, Japan

Takashi Hirose[1] (ORCID: 0000-0001-7078-4152), Hideki Ueda[1], Eisuke Fujita[1]

[1] National Research Institute for Earth Science and Disaster Resilience, Tsukuba, Ibaraki, Japan

Corresponding author: Takashi HIROSE, takashi.hirose@bosai.go.jp

Key Points:

- Waveform decorrelations in seismic ambient noise cross-correlation functions were detected repeatedly at Suwanosejima volcano, Japan.
- Repeated decorrelations were well synchronized with tilt changes, indicating magma accumulation and injection beneath Suwanosejima.
- Comparison of the amounts of decorrelation and tilt change revealed a positive correlation between them.

Abstract

The continuous estimation of changes in seismic velocity and seismic scattering property by passive interferometry using seismic ambient noise is a promising tool for monitoring volcanoes. To improve the usefulness of this method, it is necessary not only to detect subsurface structural changes but also to quantitatively compare the estimated changes in seismic wave velocity and seismic wave scattering property with other observations such as ground deformation. We applied passive interferometry to continuous seismic records from Suwanosejima volcano, Japan, recorded between April 2017 and December 2021. We detected repeated significant waveform decorrelations in seismic ambient noise cross-correlation functions, indicating seismic scattering property changes in the shallow areas of the volcano. These decorrelations were observed from 2 week to a few days before the increase in the number of explosions, suggesting that seismic scattering properties changed significantly during that period. We found that the timing of the decorrelation in seismic ambient noise cross-correlation functions and tilt changes related to magma accumulation and injection beneath Suwanosejima were well synchronized. The high correlation between the amounts of decorrelation and tilt change during the magma accumulation period suggests that a large volume of accumulated magma caused great changes in the scattering property. These results provide a significant first step toward a quantitative comparison of the amount of changes in the scattering property with the amount of magma accumulation beneath volcanoes.

Plain Language Summary

The continuous estimation of seismic velocity and seismic scattering property changes by passive interferometry using seismic ambient noise is a promising tool for monitoring volcanoes. Although many previous studies have reported seismic velocity changes related to volcanic activity, only a few of them analyzed the changes in seismic scattering properties beneath volcanoes. We compared the changes in seismic scattering property estimated by passive interferometry and ground deformation obtained from tilt records, at Suwanosejima volcano, Japan between April 2017 and December 2021. This study is the first to investigate the correlation between the temporal changes in seismic scattering properties and tilt. We detected repeated significant waveform decorrelations in seismic ambient noise cross-correlation functions, and these were well synchronized to tilt changes. Moreover, we found a positive correlation between the amounts of waveform decorrelation and tilt change observed during the magma accumulation and injection periods. These results suggest the possibility to quantitatively compare the amount of changes in the scattering property inferred from passive interferometry using seismic ambient noise with the amount of magma accumulation beneath volcanoes.

Key words: seismic scattering property change, seismic ambient noise, passive interferometry, Suwanosejima, magma accumulation

1 Introduction

The continuous estimation of seismic velocity and seismic scattering property changes by passive interferometry using seismic ambient noise (Curtis et al., 2006; Shapiro & Campillo, 2004) is a promising tool for monitoring volcanoes. Many previous studies have reported seismic velocity changes related to volcanic activity (Brenguier et al., 2008; Budi-Santoso & Lesage, 2016; Donaldson et al., 2019; Machacca-Puma et al., 2019; Nishida et al., 2020) or those associated with volcanic deformation during quiet periods (Donaldson et al., 2017; Hirose et al., 2017; Takano et al., 2017). In many cases, seismic velocity changes beneath the volcanoes have been interpreted to be because of crack opening or closing due to stress changes from magma pressurization. In some volcanoes, strain (or stress) sensitivities to seismic velocity changes have been estimated (Hirose et al., 2017; Takano et al., 2017), and the relationships between seismic velocity changes and other observations have been discussed quantitatively. Changes in seismic scattering property are observed as reductions in waveform correlations (waveform decorrelations) in seismograms. These changes originate from the emergence of new scatterers due to the injection of volcanic fluid or the creation of new cracks, which changes the properties of the medium (Larose et al., 2010; Margerin et al., 2015; Planès et al., 2015). However, there are very few studies on the changes in seismic scattering properties beneath volcanoes (Obermann et al., 2013; Sánchez-Pastor et al., 2018). Therefore, the relationship between the changes in seismic scattering properties and other observations, such as ground deformation and other surface phenomena, is poorly understood. Obermann et al. (2013) mentioned the relationship between the changes in seismic scattering properties and magma ejection volumes. They compared the ejected magma volumes of an eruption at Piton de la Fournaise on Reunion Island and the scattering cross-sections, which were computed from the decorrelation values of two eruptions in 2010. They reported that a large scattering cross-section corresponded to a large ejected magma volume. Quantitative comparison of seismic scattering property changes and other observations will be the key to developing passive monitoring tools for volcanic activities. To establish such a quantitative relationship, it is necessary to repeatedly detect changes in the seismic wave scattering characteristics of the subsurface, associated with volcanic activities, such as eruptions. However, no previous studies have focused on the repeated changes in seismic scattering properties beneath the volcanoes caused by repeated eruptions.

Suwanosejima is an active volcanic island located on the Kyushu-Ryukyu arc in the Pacific Ocean (Figure 1a). The island has an elliptical shape with major and minor axes of approximately 8 km and 6 km, respectively. In 1813–1814 and 1884–1885, eruption-extruded lava reached the western and eastern coasts of the island, respectively. A horseshoe-shaped caldera, called Mount Otake (red triangle in Figure 1a), was formed at the summit, and strombolian or vulcanian eruptions frequently occurred in a cinder cone in the caldera from 1957 to 1994 (Iguchi et al., 2008). Since the 2000s, volcanic activity at Suwanosejima has been relatively high. Eruptive activity further increased since late October 2020, and the number of eruptions increased rapidly by the end of December 2020. Volcanic activity quieted down in January and February 2021, but the number of eruptions increased again at the beginning and end of March 2021. The number of eruptions temporarily increased at the beginning and end of May 2021, June 2021, July 2021, September 2021, and December 2021 (Japan Meteorological Agency (JMA), 2022). Since December 2020, significant tilt changes in the western part of Suwanosejima associated with magma accumulation and magma injection from the western part of Suwanosejima to beneath the Otake crater have repeatedly been detected (JMA, 2022). These

magma migrations may have caused repeated changes in the subsurface structures beneath Suwanosejima.

We first attempted to detect seismic scattering property changes by passive interferometry using seismic ambient noise. Then, we explored the relationship between the changes in the scattering property and the changes in tilt related to magma migrations.

2 Data and Methods

2.1 Data

Figure 1a shows the location map of Suwanosejima volcano and the spatial distribution of the seismic stations (black x-marks). Two short-period seismometers with a natural period of 1 s were installed on the ground surface (V.SWA1, July 2001) and at a depth of 94 m (V.SWAN, August 2010), and a broadband seismometer was installed at a depth of 3 m (V.SOMS, December 2016). All seismograms were recorded at a sampling frequency of 100 Hz. We used continuous seismograms from these three seismic stations during the period April 1, 2017–December 31, 2021. All continuous seismograms are available at the Data Management Center of the National Research Institute for Earth Science and Disaster Resilience (NIED) (http://www.hinet.bosai.go.jp).

Figure 1b shows the temporal changes in the spectra of continuous seismic records from each station. We applied a fast Fourier transform to continuous seismic records every 10 min and stacked the spectra over 1 day. The significantly small spectral amplitude observed at V.SWA1 between early December 2018 and mid-May 2019 was caused by seismometer malfunction. Spectral amplitudes at frequencies between 0.5 and 1.5 Hz were relatively stable over time, whereas those above 1.5 Hz fluctuated significantly. The dominant frequency of volcanic tremors at Suwanosejima is probably approximately 2 to 6 Hz. To reduce the effect of volcanic tremors, we used seismic ambient noise records at 0.5–1 Hz (indicated by red rectangles in Figure 1b) in passive interferometry.

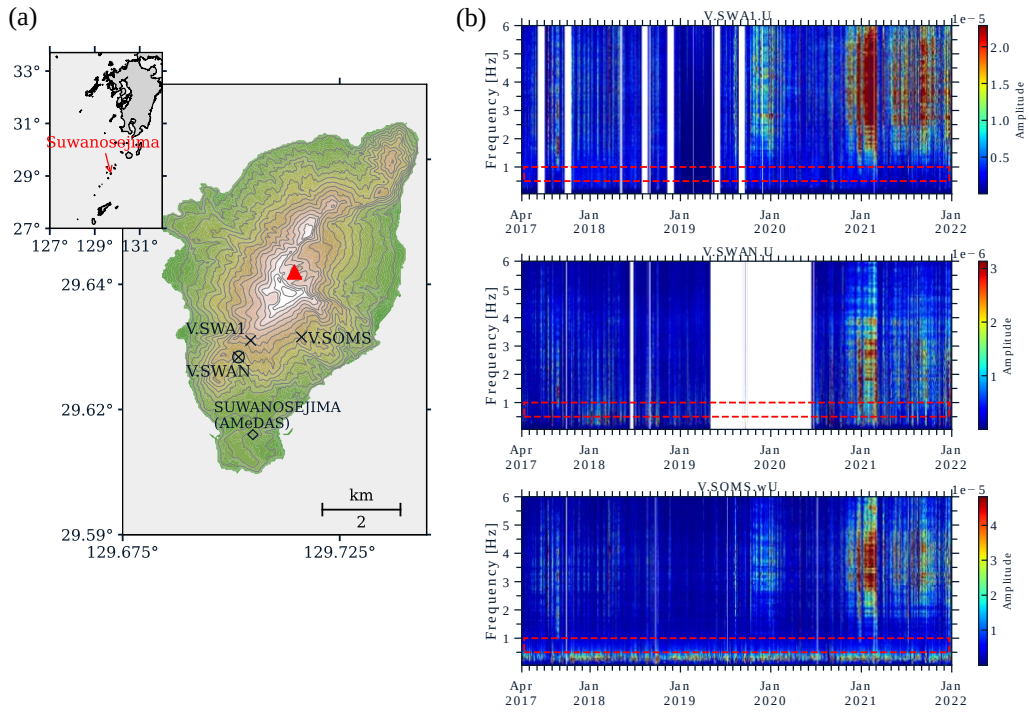

Figure 1. (a) Spatial distributions of seismometers (x-marks), tilt meter (circle), and AMeDAS (rain gauge) station (diamond). The red triangle represents the Otake crater. The ALOS Global Digital Surface Model "ALOS World 3D - 30m (AW3D30)" (https://www.eorc.jaxa.jp/ALOS/en/dataset/aw3d30/aw3d30_e.htm) was used to create the topographic map. (b) Spectrograms of continuous seismic records between April 2017 and December 2021 for each seismic station. The target frequency band of this study, 0.5–1 Hz, is indicated by red-dashed rectangles.

2.2 Estimation method of seismic scattering property changes

Cross-correlation functions (CCFs) of seismic ambient noise were computed in the frequency band 0.5–1 Hz, which had relatively stable spectral amplitudes over time. We first divided the continuous seismogram into 10-min segments and applied spectral whitening and 1-bit normalization to reduce the effect of monochromatic noise sources and transient signals with large amplitudes (Bensen et al., 2007). Then, the CCFs of seismic ambient noise were computed for every 10 min, and the daily CCFs were obtained by stacking the 10-min CCFs every day. To improve the signal-to-noise ratio of the CCFs, we stacked the daily CCFs over 3 days with a sliding time window every day (hereafter called SCCF). Figure 2 shows the SCCF waveforms for the V.SWAN–V.SOMS station pair in the 0.5- to 1-Hz band. The SCCFs were relatively stable over time, except for some periods. For example, wave packets with large amplitudes observed with a lag time between −5 and +5 s did not show seasonal variations. A similar temporal stability in the CCFs was obtained for the other station pairs. Therefore, seasonal variations in noise sources (Stehly et al., 2006) did not strongly affect the CCFs of seismic ambient noise in the 0.5-to 1-Hz band at Suwanosejima.

We applied the stretching method (Sens-Schönfelder & Wegler, 2006) to compute the waveform correlations (hereafter *CC*), which represent seismic scattering property changes and relative seismic velocity changes (hereafter *dv/v*). This method consists of simulating an artificial seismic velocity change by stretching the wavelet through a factor ε and applying the transformation $CCF(t) \rightarrow CCF((1-\varepsilon)t)$. The CCFs were stretched to several possible values of ε. The optimum *dv/v* maximized the *CC* computed between the stretched and reference CCF (RCCF) values as follows:

$$CC(\varepsilon) = \frac{\int_{t_1}^{t_2} CCF\big((1-\varepsilon)\times t\big) CCF_{ref}(t)dt}{\sqrt{\int_{t_1}^{t_2} CCF((1-\varepsilon)\times t)^2 dt \int_{t_1}^{t_2} CCF_{ref}(t)^2 dt}}. \quad (1)$$

where t_1 and t_2 represent the start and end times of the processed time window, respectively. In this study, we defined t_1 as an arrival time of direct Rayleigh wave (1.15 km/s) and $t_2 = t_1 + 15$ s. The used time window is shown by green-dashed rectangles in Figure 2. The choice of period to construct an RCCF affects the measurement of *CC* (and *dv/v*) (Sens-Schönfelder et al., 2014). The RCCF was calculated as follows: first, we calculated the *CC* values for all possible combinations of SCCFs during the study period; then, we selected the SCCFs whose average *CC* values between these in other days were greater than 0.9 to construct the RCCF. By this selection, 34–58 % of the SCCFs were excluded for each station pair. Finally, the RCCF was calculated by stacking the selected SCCFs. The calculated RCCFs were less affected by the SCCFs with low *CCs*. To compute *CC* (and *dv/v*), the stretching method was applied individually to the causal and acausal parts of the SCCF and the results were averaged.

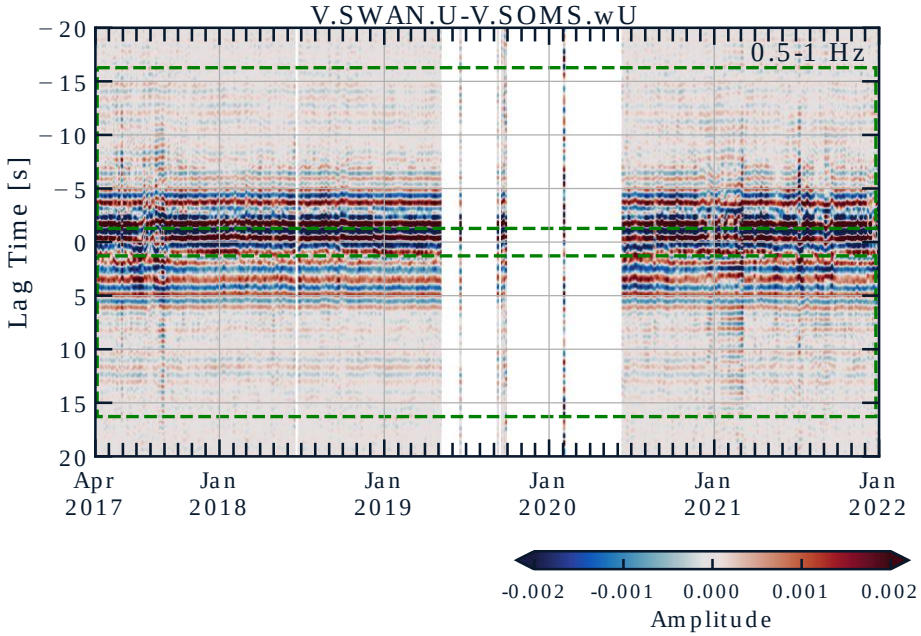

Figure 2. SCCF waveforms in the 0.5–1 Hz band for the station pair V.SWAN–V.SOMS. The portions of SCCFs represented by green-dashed rectangles were used in *dv/v* and *CC* measurements.

3 Results

Significant waveform *CC* reductions (decorrelations) in the CCFs of seismic ambient noise were observed during the study period. Figure 3 shows the temporal changes in *CC* for all pairs of stations in the 0.5- to 1-Hz band. For the V.SWAN–V.SOMS station pair, the *CC* values usually exceeded 0.9 before December 2020, except for some periods. However, significant decorrelations were observed repeatedly from mid-December 2020. *CC* values often dropped below 0.5 during this period. Similar repeated decorrelations were also estimated for the station pairs, V.SWA1–V.SOMS and V.SWA1–V.SWAN from mid-December 2020. All station pairs also showed significant repeated decorrelations during May 2017–August 2017. Repeated decorrelations were also estimated for station pair V.SWA1–V.SOMS during October 2019–February 2020. It is assumed that Rayleigh waves are predominant in the CCFs of seismic ambient noise. Therefore, these significant decorrelations indicate the changes in seismic scattering property occurred in the shallow parts of the volcano, at depths of 0–700 m. Moreover, heavy rainfall possibly causes seismic velocity or scattering property changes (Obermann et al., 2014; Rivet et al., 2015; Sens-Schönfelder & Wegler, 2006). The bottom panel of Figure 3 shows the daily precipitation at Suwanosejima. Precipitation of more than 100 mm/d was often observed at Suwanosejima during the monsoon seasons. However, repeated decorrelations did not clearly correlate with precipitation. Furthermore, temporal changes in the *CC* values did not show seasonal variations.

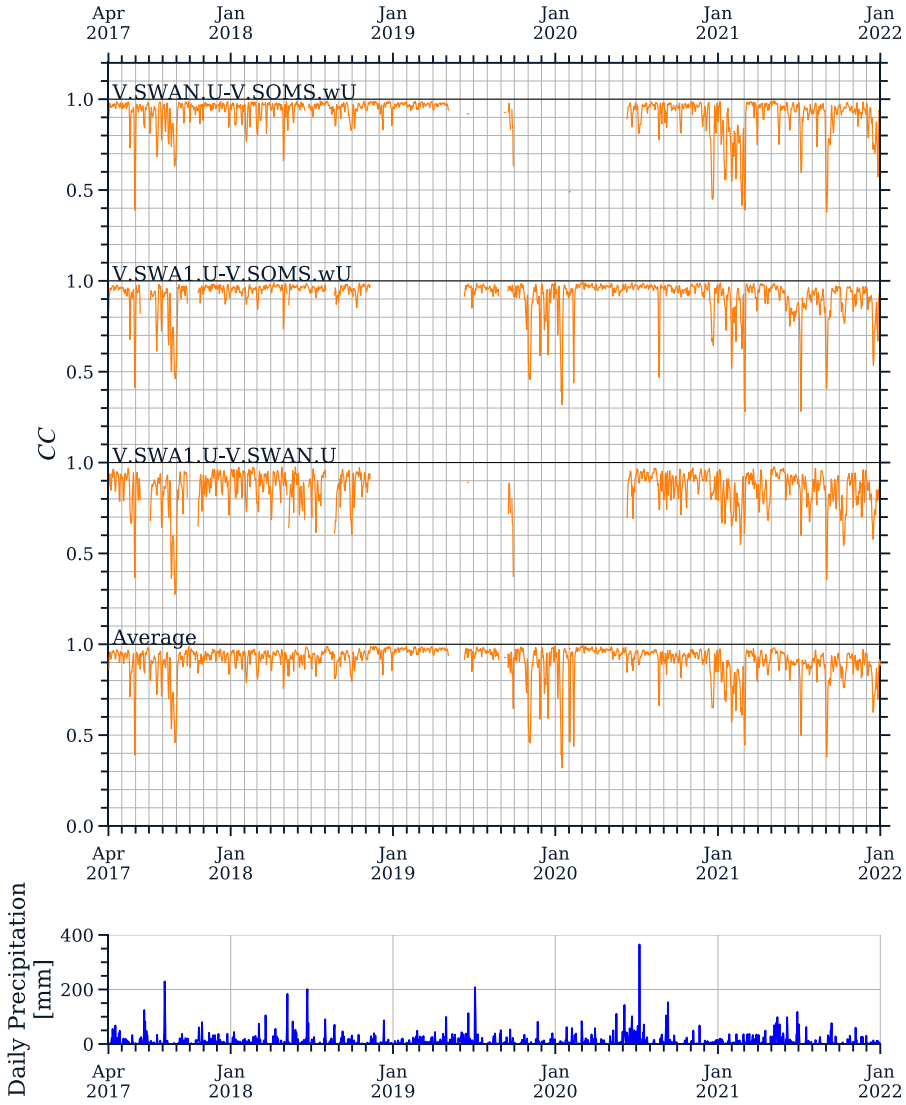

Figure 3. (top) Temporal changes in *CC* for each seismic station and the averaged one. The horizontal black lines indicate the level of *CC*=1. (bottom) Daily precipitation recorded at the AMeDAS (rain gauge) station at Suwanosejima (see Figure 1a). Precipitation data of Suwanosejima are available at https://www.data.jma.go.jp/obd/stats/etrn/index.php?prec_no=88&block_no=1654&year=&month=&day=&view=.

4 Discussion

4.1 Comparison with other observations during October 2020–December 2021

4.1.1 The number of explosions and temporal changes in waveform correlation

We first compared the number of explosions (eruptions with strong infrasound) and temporal changes in *CC* to discuss the relationship between seismic scattering property changes and volcano eruptions. At Suwanosejima, the number of explosions began to increase slightly

from October 2020. The green bars in Figure 4 indicate the number of daily explosions. An epidemic increase in the number of explosions occurred on December 21, 2020, and such a high daily activity continued for a week: 89 and 81 explosions on December 21 and 27, 2020, respectively. In 2021, there was a temporal increase in the number of explosions in almost all the months. The highest numbers of explosions, 141 and 169, were observed on December 17, 2021, and December 24, 2021, respectively. The temporal changes in the *CC* for each pair of stations and the average *CC* during the same period are shown in Figure 4. The most striking result is that an increase in the number of explosions is often accompanied by precursor decorrelations. For example, decorrelation was observed 1 week before the increased number of explosions that occurred from December 21, 2020. Similar precursory decorrelations were also detected 5 days and 14 days before the increased volcanic activities on July 6, 2021, and September 12, 2021, respectively. In most cases, the *CC*s almost recovered before the end of the temporal increase in the number of explosions. These results imply that the seismic scattering properties changed significantly before highly active explosions.

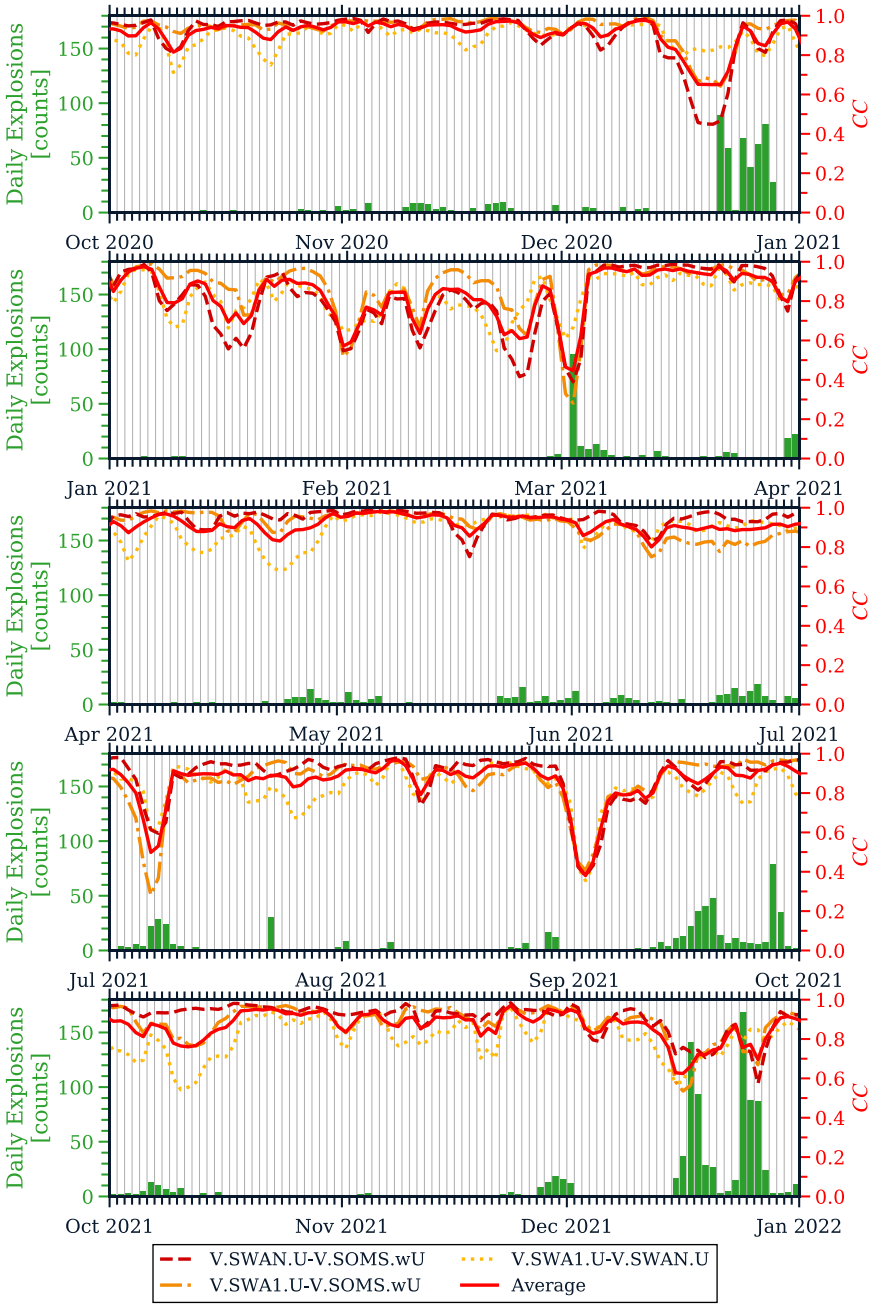

Figure 4. Daily number of explosions at Suwanosejima (green bars) and temporal changes in *CC* between October 2020 and December 2021 for each station pair (red-, orange- and yellow-dashed lines) and averaged one (red-solid line). The recent daily numbers of explosions at Suwanosejima are provided by JMA (https://www.data.jma.go.jp/svd/vois/data/fukuoka/open-data/data/511_num_data.html).

4.1.2 Temporal changes in tilt and waveform correlation

To discuss the possible cause of these decorrelations, we compared the temporal changes in the tilt and *CC*s. Figure 5a shows the east–west component of the tilt record at the V.SWAN station between October 2020 and December 2021 (see Figure 1). The tiltmeter was installed at a depth of 94 m, and the north–south and east–west components of the tilts were recorded at a sampling frequency of 1 Hz. The continuous tilt record was first decimated to hourly tilt records. The effects of tides were removed (Tamura et al., 1991) and those of rain were removed using a tank model (Kimura et al., 2015; Takagi & Onizawa, 2016; Ueda et al., 2010) (Appendix A). Significant tilt changes in the west-up and east-up components were repeatedly observed from December 2020 (indicated by the black horizontal arrows in Figure 5a). These tilt changes are interpreted as the accumulation of magma west of Suwanosejima (west-up tilt change) and injection of magma beneath the crater (east-up tilt change) (JMA, 2022). Seven magma migration periods (P1–P7) reported by JMA are marked in Figure 5a. West-up tilt changes were observed before the number of explosions increased, and east-up tilt changes were observed during highly active periods. Figure 5b shows the temporal changes in the *CC* and tilt during the magma migration periods. During P1, decorrelation and the west-up tilt change became significant from December 12, 2020, and were correlated. In the case of P2, the temporal changes in the tilt and *CC* appeared to be less correlated than those in P1. *CC* and tilt changes were well synchronized during the periods P3, P4, and P6. During P5, a clear decorrelation occurred. The timings of the largest waveform decorrelations and west-up tilt changes were almost synchronized during P3–P6. During P7, the west-up change lasted approximately 2 weeks, and a gradual decorrelation was observed during this period. In most cases, the *CC* values gradually decreased during changes in the west-up tilt and gradually recovered during changes in the east-up tilt. Thus, temporal changes in the *CC* and tilt were well correlated. This indicated that the changes in the seismic scattering property that caused changes in the CCFs of seismic ambient noise were due to magma migration beneath Suwanosejima.

The relationship between seismic velocity and ground deformation at active volcanoes has been discussed in previous studies. Donaldson et al. (2017) showed that seismic velocity changes at Kilauea volcano are well correlated with tilt changes on a time scale of days to weeks. They interpreted that such synchronized temporal changes in seismic velocity and deformation were related to the closing or opening of cracks due to deflation–inflation of the magma reservoir. Although they used seismic velocity changes and not decorrelations, their results were similar to those of this study. To our knowledge, this study is the first to investigate the correlation between temporal changes in seismic scattering properties and tilt.

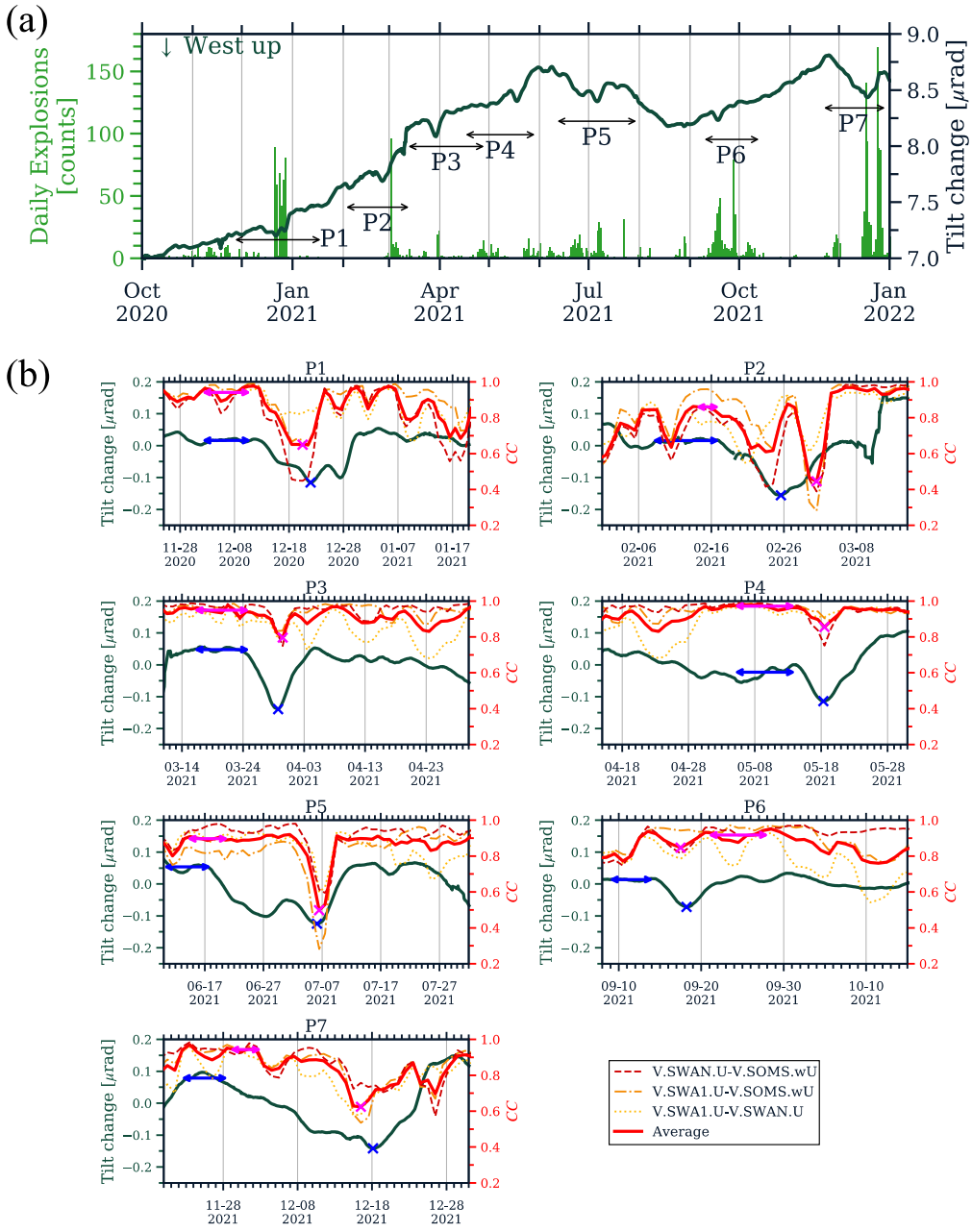

Figure 5. (a) East–west component of the tilt record at the V.SWAN station between October 2020 and December 2021. The horizontal black arrows represent periods of accumulation and injection of magma (P1–P7). The light-green bars represent the daily number of explosions. (b) Temporal changes in tilt (green lines) and *CC* (red, orange, and yellow lines) for P1–P7. Horizontal blue and magenta arrows represent periods for computing tilt and *CC* levels before changes, respectively. Blue and magenta x-marks represent the maximum tilt change and minimum *CC* levels within each period, respectively.

4.1.3 Seismic velocity changes at Suwanosejima

We estimated the temporal changes in seismic velocity (*dv/v*) using the stretching method. Figure 6 shows the temporal changes in *dv/v* for all pairs of stations in the 0.5- to 1-Hz band. The errors in the *dv/v* estimation were evaluated using the following relationship (Weaver et al., 2011):

$$rms = \frac{\sqrt{1 - CC^2}}{2CC} \sqrt{\frac{6\sqrt{\frac{\pi}{2}}T}{\omega_c^2(t_2^3 - t_1^3)}}. \quad (2)$$

where T is the inverse of the central frequency of the target frequency band, t_1 and t_2 are the start time and end time of the processed time window, respectively, $\omega_c = 2\pi f_c$ is the central angular frequency (f_c is the central frequency), and CC is the correlation value between RCCF and SCCF. Seismic velocity decreased by a few percentages for all station pairs from mid-December 2020 to February 2021. Further, seismic velocity decreased between July and August 2017 for all pairs of stations. However, in the case of seismic velocities, the common temporal changes between all pairs of stations were less prominent than those in the *CCs*. The uncertainty in the estimated *dv/v* becomes high in the case of a low *CC* (Equation 2). Daily precipitation (bottom panel of Figure 6) and *dv/v* did not appear to be correlated.

We compared the temporal changes in *dv/v* and tilt, as we did for *CC* changes. Figure 7 shows a comparison between the changes in tilt and *dv/v* for the periods of magma migration (P1–P7). Temporal changes in tilt and *dv/v* were correlated during P1 and P5. However, the correlations were less significant than in the case of changes in tilt and *CC*. We suggest three possible interpretations for this low correlation between temporal changes in *dv/v* and tilt. First, an unstable estimation of *dv/v* led to a low correlation. As mentioned above, the uncertainty in a *dv/v* computation depends on the waveform correlation, *CC* (Equation 2). During magma accumulation and injection, significant decorrelations were detected, which might have affected the *dv/v* computation. The second interpretation is that the region of subsurface structural changes due to magma migration did not extend widely. Previous studies located change regions in seismic velocities whose sizes of larger than the wavelength (e.g., Brenguier et al., 2008; Obermann et al., 2013; Machacca-Puma et al., 2019). In our case, the wavelength of Rayleigh waves ranges 1.15–1.5 km. The third interpretation is that seismic velocity changes are less sensitive to fluid injection compared to waveform decorrelations. In a laboratory experiment by measuring *dv/v* and *CC*, Théry et al. (2020) demonstrated that decorrelations were more sensitive to the injection of fluid into a porous medium as the amount of injected water increases. Recently, Tonegawa et al. (2022) succeeded in detecting waveform decorrelations in seismic ambient noise CCFs before and during slow earthquakes in the Nankai accretionary prism, Japan. They interpreted that those decorrelations were caused by fluid migrations. In their results, temporal changes in *CC* are more correlated to occurrences of slow earthquakes than those in seismic velocities. Based on the differences in the temporal changes (spatiotemporal changes) of *dv/v* and *CC*, further studies are needed to clarify in detail the factors that cause subsurface structural changes. Simultaneous computations of *dv/v* and *CC* for various regions, both volcanic and non-volcanic, are important to access these points.

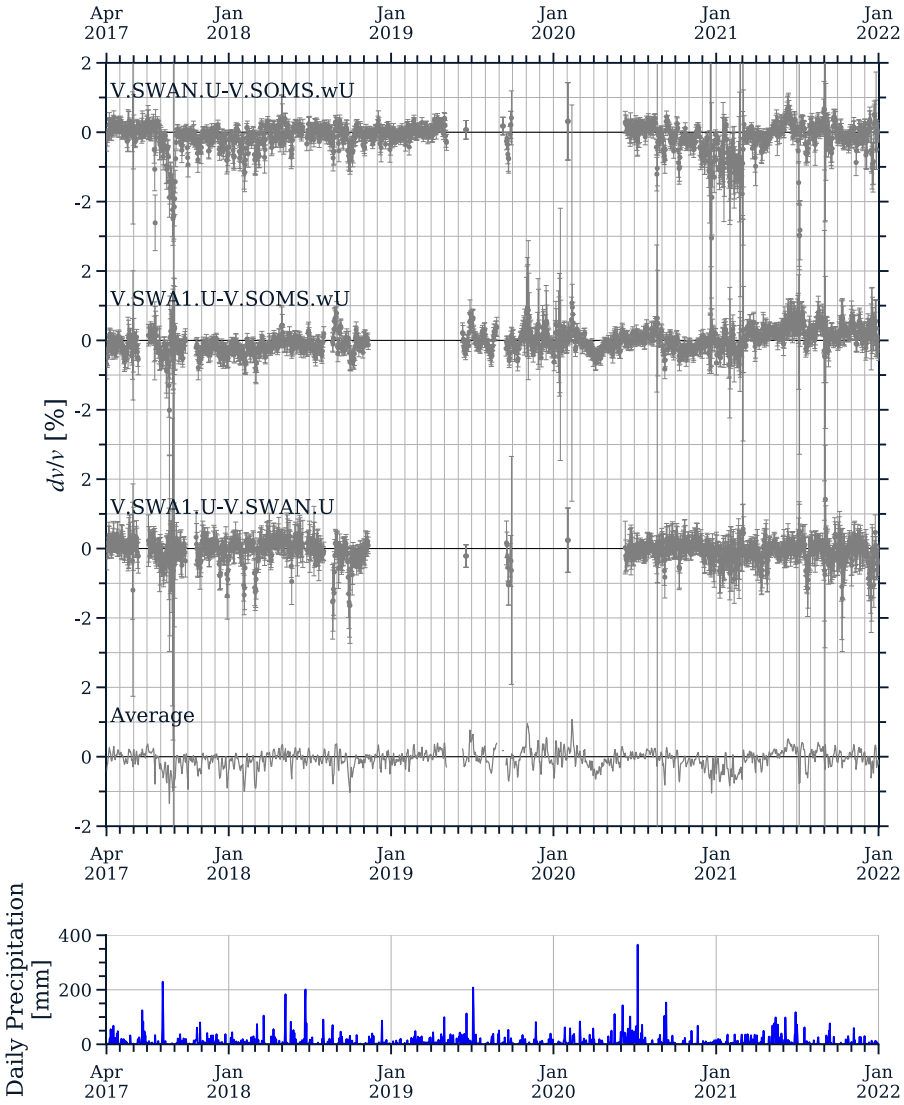

Figure 6. (top) Temporal changes in *dv/v* for each seismic station and the averaged one. (bottom) Daily precipitation recorded at the AMeDAS station.

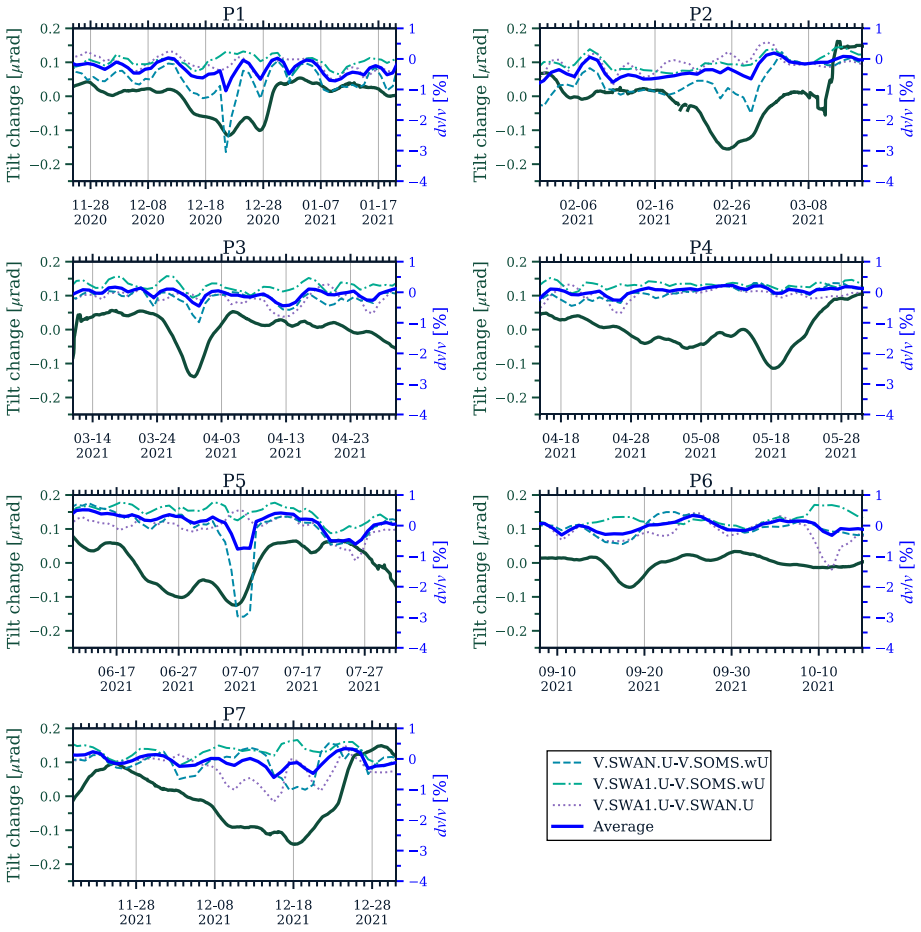

Figure 7. Temporal changes in tilt (green lines) and *dv/v* (blue, green, and purple lines) for P1–P7.

4.2 Correlation between CC and tilt changes throughout the study period

In the previous section, we showed the synchronized changes in *CC* and tilt for the periods of magma migration from October 2020 (P1–P7). Here, we computed these correlations throughout the study period to estimate the correlations between the temporal changes in *CC* and tilt before October 2020. Figure 8a shows the temporal changes in *CC* averaged over all three station pairs (red line) and the east–west component of the tilt record at V.SWAN (green line), between April 2017 and December 2021. Figure 8b shows the temporal changes in the correlation functions between the *CC* and changes in tilt for three different (11-day, 21- day, 31-day) time windows. We computed them by sliding the time window for every day. We defined the tilt changes as a reference; therefore, a positive lag time means that a *CC* change is delayed to tilt changes. As it is difficult to determine the suitable length for the time window, we estimated the results on three different time windows. Before calculating the correlation functions between the *CC* and tilt, the hourly tilt records were averaged and decimated to daily records. Changes in *CC* and tilt were well correlated during the periods P1–P7 and are indicated

by black horizontal bars in Figure 8. For these periods, the maximum amplitudes of the correlation functions exceeded 0.7. Such periods of high correlation between *CC* and tilt changes were also estimated in 2017 and 2018, as indicated by the black horizontal bars (hereafter called P8–P12) in Figure 8. Although a similar high correlation between *CC* and tilt changes was detected during June–August 2020, tilt records in these periods were highly scattered, and it was difficult to compare the *CC* and tilt changes. Therefore, we did not use these periods in this study.

Figure 9 shows the temporal changes in tilt and *CC* for the periods P8–P12. The timings of the decorrelation and tilt changes were well synchronized. During P8, the *CC* value fell significantly from 0.95 to 0.4, although the changes in tilt were not higher than those in other periods. To estimate the difference in SCCF for P8 and those for other periods, we computed the similarities between the waveforms using the stretching method. Figure 10 shows the correlation matrix of SCCFs for P1–P12 for the V.SWAN–V.SOMS station pair. The SCCFs for the days with the lowest *CCs* within each period were used for the computation. The SCCF for P8 showed a very low correlation with the SCCF for other periods. The decorrelation observed for P8 might not be related to magma accumulation and injection beneath Suwanosejima; other factors might have caused this decorrelation. Although the JMA did not report P9–P12 as magma accumulation and injection periods in 2017 and 2018, changes in the scattering property similar to P1–P7 could also have occurred in P9–P12.

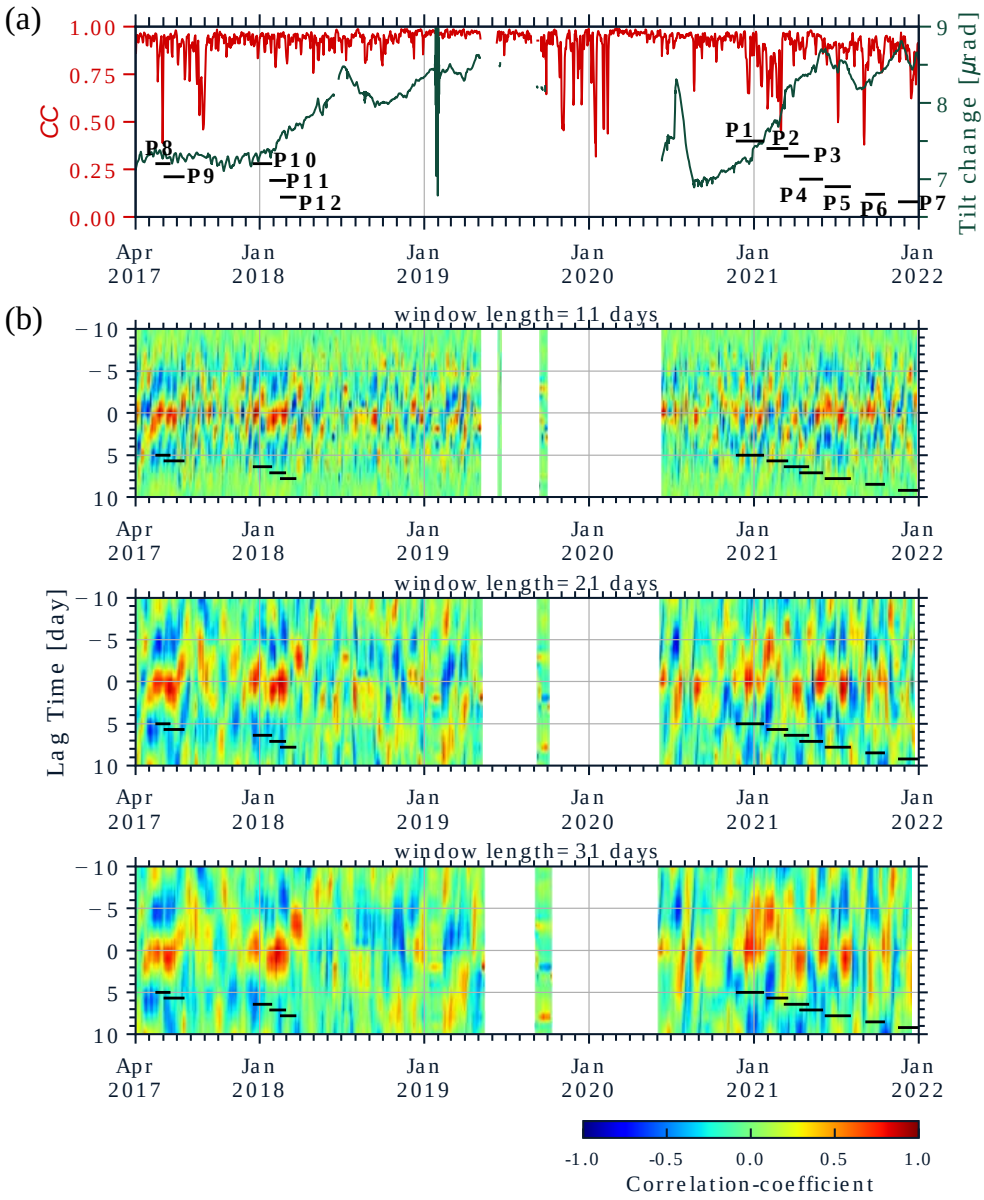

Figure 8. (top) Temporal changes in *CC* averaged for all station pairs (red line) and tilt record on the east–west component at the station V.SWAN (green line) between April 2017 and December 2021. The horizontal black bars correspond to magma accumulation and injection periods (P1–P7) and other periods for which the changes in CC and tilt show a high correlation (P8–P12).

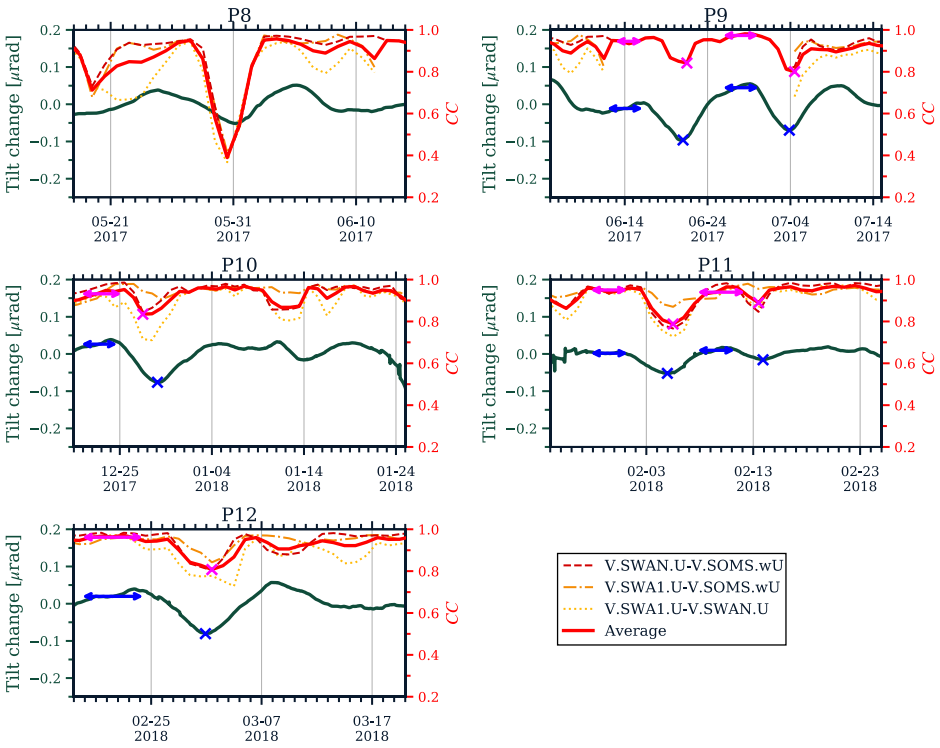

Figure 9. Similar to Figure 5b, but for P8–P12.

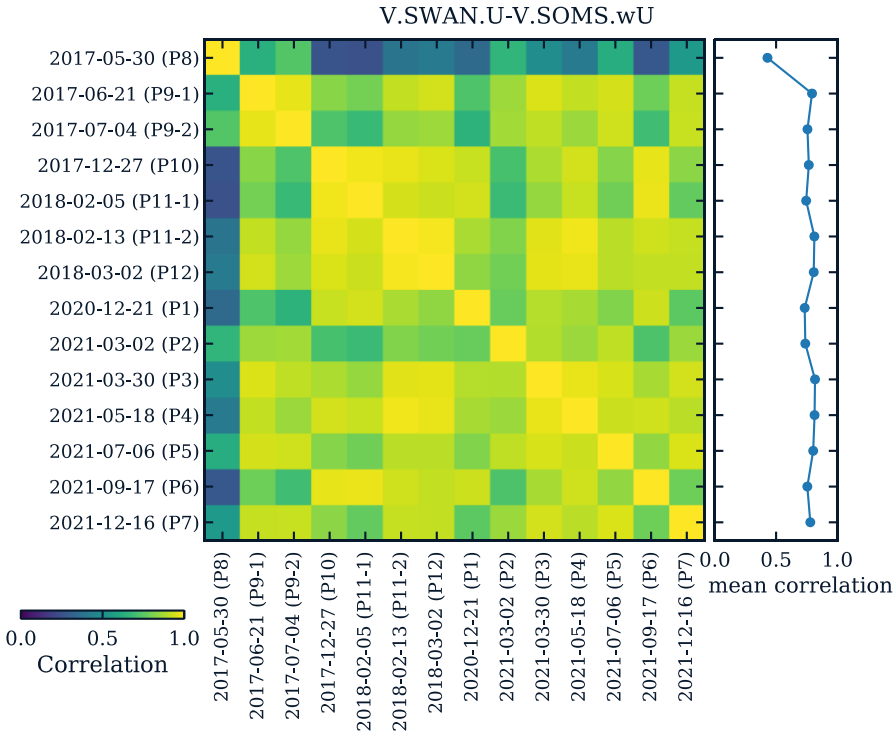

Figure 10. A correlation matrix of SCCFs for P1–P12 for the V.SWAN-V.SOMS station pair.

4.3 Relationship between amounts of decorrelation and tilt change

Comparing the amounts of decorrelation and tilt change will contribute to improving volcano monitoring with seismic scattering property changes. Here, we compared the amounts of decorrelation and tilt change observed during the magma migration periods. We defined the amount of decorrelation as the difference between the *CC* level in the period before the decorrelation corresponding to the tilt change occurred and the *CC* value when the *CC* dropped the most. For example, during P1, the decorrelation corresponding to the tilt change occurred once (see Figure 5b). The median *CC* level in the period indicated by the horizontal magenta arrow was assumed to be the *CC* level before the change and that indicated by the magenta x-mark to be the minimum *CC* level. The average CC values of all three station pairs were used in the calculations. The amount of tilt change for P1 was defined as the difference between the amount of tilt before the change (blue horizontal arrows in Figure 5b) and the amount of tilt when the tilt from east to west was at its maximum (blue x mark in Figure 5b). The amounts of decorrelation and tilt changes for P2–P7 and P9–P12 were computed using the same procedure. The decorrelation event during P8 was not used because the decorrelation in this period was attributed to a different factor than that in the other periods. Figure 11 shows the relationship between the amounts of decorrelation and the change in tilt for the 13 data points from P1 to P7 and P9 to P12. Large tilt changes appeared to cause large decorrelation. The correlation coefficient was 0.76 (p-value = 0.003). The amounts of decorrelation and tilt changes in P9–P12 were smaller than those in P1–P3, P5, and P7. The number of explosions in P9–P12 was significantly lower than that in P1–P3, P5, and P7. Therefore, the activity level of the surface phenomena might correlate with the amount of decorrelation.

Obermann et al. (2013) compared the ejected magma volumes of an eruption at Piton de la Fournaise on Reunion Island and the scattering cross sections, which were computed from the decorrelation values for the two eruptions in 2010. They reported that a large scattering cross section corresponded to a large magma volume and that the ejected magma volume was of the order of the cubic value of the scattering cross section. No further studies have discussed this type of scaling relationship in active volcanoes. Although Obermann et al. (2013) used only two events, their study inspired us to investigate the repeated occurrence of decorrelations at Suwanosejima that were synchronized with the tilt changes and to discuss the relationship between the amounts of tilt change and decorrelation using a large data set.

The following is a summary of the phenomena that might have occurred beneath the Suwanosejima volcano during P1–P7 and P9–P12:

(1) *Magma accumulation period*: Magma accumulation occurred in the shallow areas of Suwanosejima, and this accumulation caused a west-up tilt change at the V.SWAN station. The scattering property of the subsurface area around the magma accumulation changed significantly, and this caused waveform changes (decorrelations) in the CCFs of seismic ambient noise. The west-up tilt change at the V.SWAN station indicated an accumulation of magma on the western part of Suwanosejima. We assume that the accumulation of magma occurs below 1 km depth because the penetration depth of Rayleigh waves at 0.5–1 Hz is approximately 700 m.

(2) *Magma injection period*: After the accumulation of magma in the shallow parts of western Suwanosejima, the magma was injected beneath the crater. This was indicated by the east-up tilt change at the V.SWAN station. The number of explosions increased during this period. As magma accumulated in the previous stage moved beneath the crater and was emitted by

eruptions, the *CC* value of the CCFs of seismic ambient noise was recovered. Observations in these two stages suggest that the changes in the CCFs of seismic ambient noise, caused by changes in the scattering properties, were due to magma accumulation in the shallow parts of western Suwanosejima.

The high correlation between the amounts of decorrelation and tilt change suggests that a large volume of magma accumulated during the *magma accumulation period* caused great changes in the scattering property. At present, it is difficult to discuss in detail the relationships between the amount of decorrelation and the accumulated magma volume because the spatial distribution of the changes in the scattering property and the parameters of the pressure sources (location, geometry, and amount of volume change) obtaining from geodetic data are not available for Suwanosejima. However, the results of this study suggest the possibility to quantitatively compare the amount of changes in the scattering property inferred from passive interferometry using seismic ambient noise with the amount of magma accumulation beneath volcanoes.

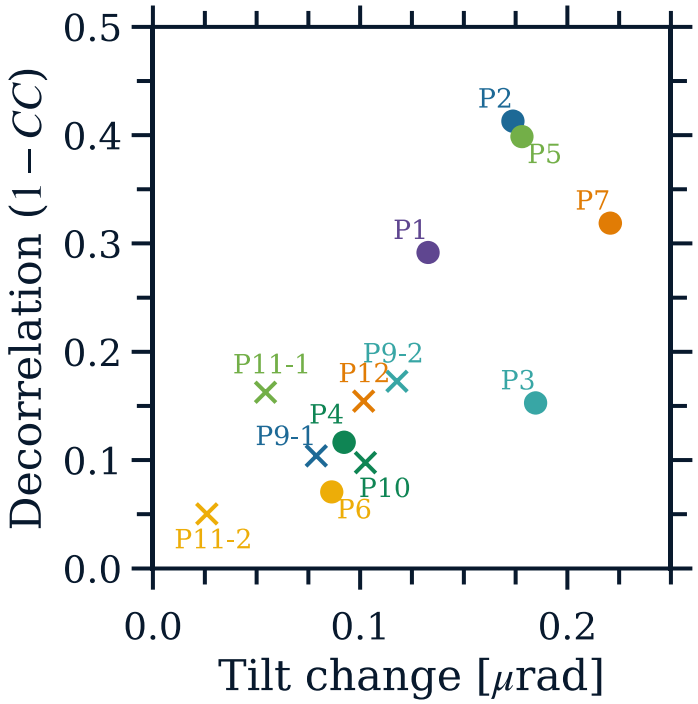

Figure 11. A relationship between the amounts of decorrelation (1-*CC*) and tilt change. The results for P1–P7 are indicated by closed circles, and those for P9–P12 are indicated by x-marks. Some periods include two or three decorrelation events. For example, P9-1 and P9-2 mean the first and second decorrelation events in P9 (see also Figure 9), respectively.

5 Conclusion

We applied passive interferometry to continuous seismic records from Suwanosejima volcano, Japan, recorded during April 2017–December 2021. We detected repeated significant reductions in waveform correlation (waveform decorrelations) in seismic ambient noise CCFs,

indicating seismic scattering property changes in the shallow parts of the volcano. These decorrelations started from 2 weeks to few days before the increase in the number of explosions, suggesting that seismic scattering properties changed significantly before highly active explosions. Further, we found that the timing of the waveform decorrelation in seismic ambient noise CCFs and tilt changes, related to magma accumulation and injection beneath Suwanosejima, were well synchronized. Magma accumulations in the western part of Suwanosejima were detected as west-up tilt changes and probably caused seismic scattering property changes. Magma injections beneath the crater were detected as east-up tilt changes and caused recovery in waveform correlations. Repeated occurrence of decorrelations at Suwanosejima that were synchronized with the tilt changes allowed us to discuss the relationship between the amounts of decorrelation and tilt change. The high correlation between the amounts of decorrelation and tilt change suggests that the large volume of accumulated magma caused great changes in the scattering property. Further detailed discussion is limited because the spatial distribution of the changes in the scattering property and the parameters of the pressure sources obtained from geodetic data are not available for Suwanosejima. However, our results are the first to show a high correlation between the temporal changes in seismic scattering properties and tilt and provide a significant first step toward quantitative comparison of the amount of changes in the scattering property with the amount of magma accumulation beneath volcanoes.

Acknowledgments

We thank the Japan Meteorological Agency (JMA) for providing seismograms, tilt records, a list of the number of explosions, and precipitation data. T.H. was supported by JSPS KAKENHI, Grant 20K14581.

Open Research

Continuous seismograms and tilt records are available from the Data Management Center of the NIED (http://www.hinet.bosai.go.jp). Precipitation data at the AMeDA station at Suwanosejima maintained by the JMA are available at https://www.data.jma.go.jp/obd/stats/etrn/index.php?prec_no=88&block_no=1654&year=&month=&day=&view=. The recent daily number of explosions at Suwanosejima was provided by the JMA (https://www.data.jma.go.jp/svd/vois/data/fukuoka/open-data/data/511_num_data.html). The DEM data, ALOS Global Digital Surface Model "ALOS World 3D - 30m (AW3D30)," used to create a topographic map, are available at https://www.eorc.jaxa.jp/ALOS/en/dataset/aw3d30/aw3d30_e.htm.

Appendix

A1. Correction of rain effects in tilt records

The tilt changes caused by rainfall are among the largest noises in the tilt records. At Suwanosejima, more than 100 mm of precipitation is often observed daily during the monsoon season. Such heavy rains were also observed during magma accumulation and injection periods. To improve our comparison of temporal changes in tilt and *CC* (*dv/v*), we corrected for precipitation effects in the tilt records.

A tank model consisting of three vertically connected tanks was used (Figure A1). Each tank corresponded to an aquifer at different depths. The downward force due to the load on each tank was assumed to be proportional to the water level, and the tilt variation due to the load was assumed to be proportional to the force as in the case of a semi-infinite homogeneous elastic body. The tilt record was corrected using a model combined with a first-order delay system. In the tank model, the water level at time t_n in the *i*-th aquifer, $y_i(t_n)$, is expressed as follows:

$$y_i(t_{n+1}) = \begin{cases} (1-r_i)y_i(t_n) + P(t_n) & \text{for} \quad i = 1 \\ (1-r_j)y_i(t_n) + r_{i-1}y_{i-1}(t_n) & \text{for} \quad i \neq 1. \end{cases} \qquad (A1)$$

where r_i represents the penetration rate of the *i*-th aquifer and $P(t_n)$ represents precipitation at time t_n. The first layer was directly affected by rainfall. In this study, we corrected hourly tilt records using hourly precipitation data recorded at the AMeDAS station at Suwanosejima. The synthetic tilt change ΔT caused by rainfall was calculated as the sum of the loading from each aquifer:

$$\Delta T(t_n) = \sum_{i=1}^{3} A_i y_i(t_n). \qquad (A2)$$

Here, A_i is a constant value that is determined by fitting the synthetic tilt changes to the observed values between August 1 and August 15, 2017 (light-green curve in Figure A2). Note that the effects of tides were already removed in that observed tilt (Tamura et al., 1991). During this period, only a few eruptions occurred; thus, we expect that tilt changes during this period were mainly caused by heavy rainfall.

The best-fit values of A_i and r_i (*i*=1,2,3) were determined using a grid search. The search ranges of A_i and r_i were –0.05 to 0.05 and 0.001–0.5, respectively. The best-fit values were determined to be $(A_1, A_2, A_3) = (-0.0005, 0.0001, -0.005)$ and $(r_1, r_2, r_3) = (0.1, 0.01, 0.05)$. The gray curve in Figure A2 represents ΔT from the best-fit values of A_i and r_i. This synthesized tilt change almost explains the largest tilt change around August 7, 2017, in the original tilt record (light-green curve). The dark-green curve in Figure A2 represents the tilt changes after subtracting the tilt changes synthesized by the tank model from the original tilt record. Although we used a simple tank model, the effects of heavy rain were almost completely eliminated. Finally, we corrected the tilt records of the study period using a tank model with the same A_i and r_i. The tilt changes shown in Figures 5, 7, 8, and 9 were those after removing the effects of rainfall.

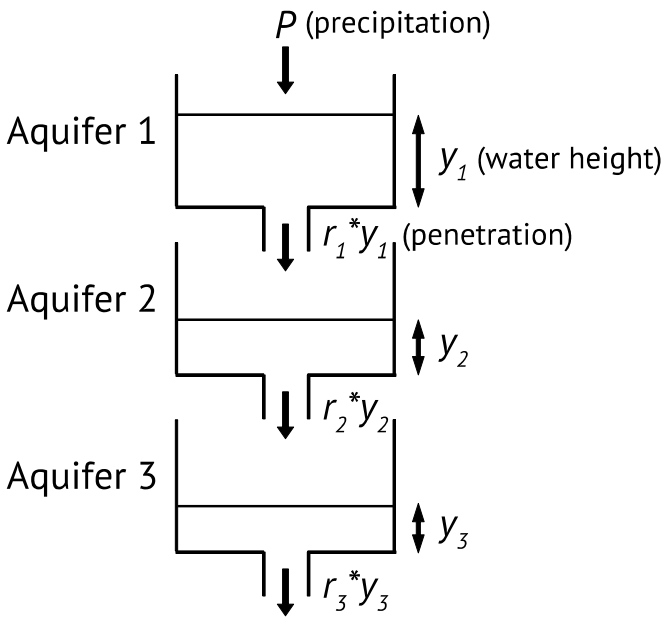

Figure A1. A schematic illustration of the tank model.

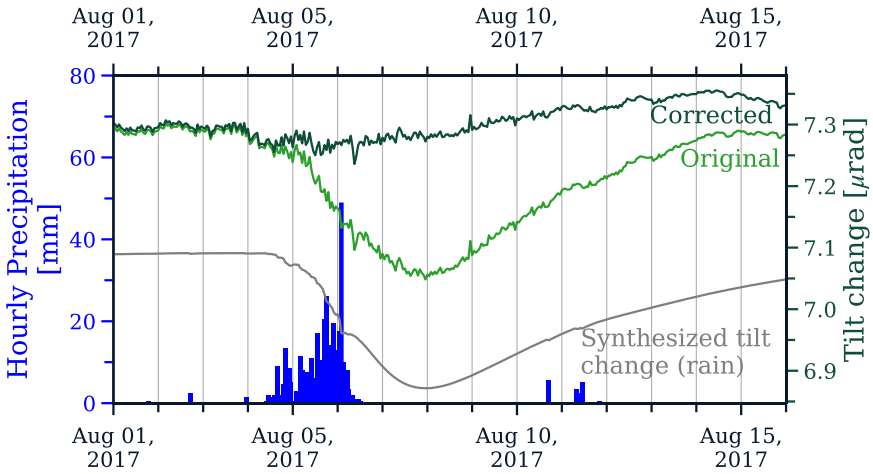

Figure A2. Tilt records after removing the tide effect (light-green line), after removing the tide and rain effects (dark-green line), and the synthesized tilt change due to rain (gray line) between August 1, 2017, and August 15, 2017. The blue bars represent the hourly precipitations.

References

Bensen, G. D., Ritzwoller, M. H., Barmin, M. P., Levshin, A. L., Lin, F., Moschetti, M. P., et al. (2007). Processing seismic ambient noise data to obtain reliable broad-band surface wave dispersion measurements. *Geophysical Journal International*, 169(3), 1239–1260. https://doi.org/10.1111/j.1365-246X.2007.03374.x

Brenguier, F., Shapiro, N. M., Campillo, M., Ferrazzini, V., Duputel, Z., Coutant, O., & Nercessian, A. (2008). Towards forecasting volcanic eruptions using seismic noise. *Nature Geoscience*, 1(2), 126–130. https://doi.org/10.1038/ngeo104

Budi-Santoso, A., & Lesage, P. (2016). Velocity variations associated with the large 2010 eruption of Merapi volcano, Java, retrieved from seismic multiplets and ambient noise cross-correlation. *Geophysical Journal International*, 206(1), 221–240. https://doi.org/10.1093/gji/ggw145

Curtis, A., Gerstoft, P., Sato, H., Snieder, R., & Wapenaar, K. (2006). Seismic interferometry—turning noise into signal. *Leading Edge*, 25(9), 1082–1092. https://doi.org/10.1190/1.2349814

Donaldson, C., Caudron, C., Green, R. G., Thelen, W. A., & White, R. S. (2017). Relative seismic velocity variations correlate with deformation at Kīlauea volcano. Science Advances, 3(6), e1700219. https://doi.org/10.1126/sciadv.1700219

Donaldson, C., Winder, T., Caudron, C., & White, R. S. (2019). Crustal seismic velocity responds to a magmatic intrusion and seasonal loading in Iceland's Northern Volcanic Zone. *Science Advances*, 5(11), eaax6642. https://doi.org/10.1126/sciadv.aax6642

Hirose, T., Nakahara, H., & Nishimura, T. (2017). Combined use of repeated active shots and ambient noise to detect temporal changes in seismic velocity: application to Sakurajima volcano, Japan. *Earth, Planets and Space*, 69(1), 1–12. https://doi.org/10.1186/s40623-017-0613-7

Iguchi, M., Yakiwara, H., Tameguri, T., Hendrasto, M., & Hirabayashi, J.-I. (2008). Mechanism of explosive eruption revealed by geophysical observations at the Sakurajima, Suwanosejima and Semeru volcanoes. *Journal of Volcanology and Geothermal Research*, 178(1), 1–9. https://doi.org/10.1016/j.jvolgeores.2007.10.010

Japan Meteorological Agency (2022) (2-2) Suwanosejima. Documents for the 149th meeting of the coordinating committee for prediction of volcanic eruptions (in Japanese) Accessed 17 February 2022. Retrieved from https://www.data.jma.go.jp/svd/vois/data/tokyo/STOCK/kaisetsu/CCPVE/shiryo/149/149_2-2.pdf

Kimura, K., Tsuyuki, T., Suganuma, I., Hasegawa, H., Misu, H., & Fujita, K. (2015). Rainfall Correction of Volumetric Strainmeter Data by Tank Models. *Q J Seismol*, 78, 93–158.

Larose, E., Planes, T., Rossetto, V., & Margerin, L. (2010). Locating a small change in a multiple scattering environment. *Applied Physics Letters*, 96(20). https://doi.org/10.1063/1.3431269

Machacca-Puma, R., Lesage, P., Larose, E., Lacroix, P., & Anccasi-Figueroa, R. M. (2019). Detection of pre-eruptive seismic velocity variations at an andesitic volcano using ambient noise correlation on 3-component stations: Ubinas volcano, Peru, 2014. *Journal of Volcanology and Geothermal Research*, 381, 83–100. https://doi.org/10.1016/j.jvolgeores.2019.05.014

Margerin, L., Planès, T., Mayor, J., & Calvet, M. (2015). Sensitivity kernels for coda-wave interferometry and scattering tomography: theory and numerical evaluation in two-dimensional anisotropically scattering media. *Geophysical Journal International*, 204(1), 650–666. https://doi.org/10.1093/gji/ggv470

Nishida, K., Mizutani, Y., Ichihara, M., & Aoki, Y. (2020). Time-lapse monitoring of seismic velocity associated with 2011 shinmoe-dake eruption using seismic interferometry: An extended Kalman filter approach. *Journal of Geophysical Research:Solid Earth*, 125(9). https://doi.org/10.1029/2020jb020180

Obermann, A., Froment, B., Campillo, M., Larose, E., Planès, T., Valette, B., et al. (2014). Seismic noise correlations to image structural and mechanical changes associated with the M w 7.9 2008 Wenchuan earthquake. *Journal of Geophysical Research:Solid Earth*, 119(4), 3155–3168. https://doi.org/10.1002/2013jb010932

Obermann, A., Planès, T., Larose, E., & Campillo, M. (2013). Imaging preeruptive and coeruptive structural and mechanical changes of a volcano with ambient seismic noise. *Journal of Geophysical Research:Solid Earth*, 118(12), 6285–6294. https://doi.org/10.1002/2013jb010399

Planès, T., Larose, E., Rossetto, V., & Margerin, L. (2015). Imaging multiple local changes in heterogeneous media with diffuse waves. *The Journal of the Acoustical Society of America*, 137(2), 660–667. https://doi.org/10.1121/1.4906824

Rivet, D., Brenguier, F., & Cappa, F. (2015). Improved detection of preeruptive seismic velocity drops at the Piton de La Fournaise volcano. *Geophysical Research Letters*, 42(15), 6332–6339. https://doi.org/10.1002/2015gl064835

Sánchez-Pastor, P., Obermann, A., & Schimmel, M. (2018). Detecting and locating precursory signals during the 2011 El Hierro, canary islands, submarine eruption. *Geophysical Research Letters*, 45(19), 10,288–10,297. https://doi.org/10.1029/2018gl079550

Sens-Schönfelder, C., Pomponi, E., & Peltier, A. (2014). Dynamics of Piton de la Fournaise volcano observed by passive image interferometry with multiple references. *Journal of Volcanology and Geothermal Research*, 276, 32–45. https://doi.org/10.1016/j.jvolgeores.2014.02.012

Sens-Schönfelder, C., & Wegler, U. (2006). Passive image interferometry and seasonal variations of seismic velocities at Merapi Volcano, Indonesia. *Geophysical Research Letters*, 33(21). https://doi.org/10.1029/2006gl027797

Shapiro, N. M., & Campillo, M. (2004). Emergence of broadband Rayleigh waves from correlations of the ambient seismic noise. *Geophysical Research Letters*, 31(7). https://doi.org/10.1029/2004gl019491

Stehly, L., Campillo, M., & Shapiro, N. M. (2006). A study of the seismic noise from its long-range correlation properties. *Journal of Geophysical Research*, 111(B10). https://doi.org/10.1029/2005jb004237

Takano, T., Nishimura, T., & Nakahara, H. (2017). Seismic velocity changes concentrated at the shallow structure as inferred from correlation analyses of ambient noise during volcano deformation at Izu-Oshima, Japan. *Journal of Geophysical Research:Solid Earth*, 122(8), 6721–6736. https://doi.org/10.1002/2017jb014340

Takagi, A., & Onizawa, S. (2016). Shallow pressure sources associated with the 2007 and 2014 phreatic eruptions of Mt. Ontake, Japan. *Earth, Planets and Space*, 68(1), 1–9. https://doi.org/10.1186/s40623-016-0515-0

Tamura, Y., Sato, T., Ooe, M., & Ishiguro, M. (1991). A procedure for tidal analysis with a Bayesian information criterion. *Geophysical Journal International*, 104(3), 507–516. https://doi.org/10.1111/j.1365-246X.1991.tb05697.x

Théry, R., Guillemot, A., Abraham, O., & Larose, E. (2020). Tracking fluids in multiple scattering and highly porous materials: Toward applications in non-destructive testing and seismic monitoring. *Ultrasonics*, 102, 106019. https://doi.org/10.1016/j.ultras.2019.106019

Tonegawa, T., Takemura, S., Yabe, S., & Yomogida, K. (2022). Fluid migration before and during slow earthquakes in the shallow Nankai subduction zone. *Journal of Geophysical Research:Solid Earth*, 127(3). https://doi.org/10.1029/2021jb023583

Ueda, H., Fujita, E., Ukawa, M., & Yamamoto, E. (2010). Automated Technique for Anomalous Volcanic Crustal Deformation Detection and Source Estimation by Using Real Time Tiltmeter Data. *Report of the National Research Institute for Earth Science and Disaster Prevention*, 76, 21–32.

Weaver, R. L., Hadziioannou, C., Larose, E., & Campillo, M. (2011). On the precision of noise correlation interferometry. *Geophysical Journal International*, 185(3), 1384–1392. https://doi.org/10.1111/j.1365-246X.2011.05015.x